J Biol Inorg Chem (2004) 9: 997–1006
DOI 10.1007/s00775-004-0601-9

ORIGINAL ARTICLE

**Paola Caroppi · Federica Sinibaldi · Elisa Santoni
Barry D. Howes · Laura Fiorucci · Tommaso Ferri
Franca Ascoli · Giulietta Smulevich · Roberto Santucci**

The 40s Ω-loop plays a critical role in the stability and the alkaline conformational transition of cytochrome *c*

Received: 1 July 2004 / Accepted: 14 September 2004 / Published online: 19 October 2004

The structural and redox properties of a non-covalent complex reconstituted upon mixing two non-contiguous fragments of horse cytochrome *c*, the residues 1–38 heme-containing N-fragment with the residues 57–104 C-fragment, have been investigated. With respect to native cyt *c*, the complex lacks a segment of 18 residues, corresponding, in the native protein, to an omega (Ω)-loop region. The fragment complex shows compact structure, native-like α-helix content but a less rigid atomic packing and reduced stability with respect to the native protein. Structural heterogeneity is observed at pH 7.0, involving formation of an axially misligated low-spin species and consequent partial displacement of Met80 from the sixth coordination position of the heme-iron. Spectroscopic data suggest that a lysine (located in the Met80-containing loop, namely Lys72, Lys73, or Lys79) replaces the methionine residue. The residues 1–38/57–104 fragment complex shows an unusual biphasic alkaline titration characterized by a low ($pK_{a1} = 6.72$) and a high pK_a-associated state transition ($pK_{a2} = 8.56$); this behavior differs from that of native cyt *c*, which shows a monophasic alkaline transition ($pK_a = 8.9$). The data indicate that the 40s Ω-loop plays an important role in the stability of cyt *c* and in ensuring a correct alkaline conformational transition of the protein.

P. Caroppi · F. Sinibaldi · L. Fiorucci · F. Ascoli
R. Santucci (✉)
Dipartimento di Medicina Sperimentale e Scienze Biochimiche,
Università di Roma "Tor Vergata",
via Montpellier 1, 00133 Rome, Italy
E-mail: santucci@med.uniroma2.it
Fax: +39-06-72596353

E. Santoni · B. D. Howes · G. Smulevich
Dipartimento di Chimica,
Università di Firenze,
via della Lastruccia 3,
50019 Sesto Fiorentino, Italy

T. Ferri
Dipartimento di Chimica,
Università di Roma "La Sapienza",
P. le A. Moro 5, 00185 Rome, Italy

Keywords Cytochrome *c* · Fragment complex · Intermediate state · Loop regions

Abbreviations CD: circular dichroism · CV: cyclic voltammetry · cyt *c*: cytochrome *c* · RR: resonance Raman

Introduction

The structural and functional characterization of intermediate states represents an interesting tool to better understand protein folding pathways [1, 2, 3, 4, 5]. An interesting approach for studying partly folded states of proteins is based on the use of limited proteolysis [6]. Protein structure is composed of sub-domains connected by flexible hinges; under appropriate conditions the polypeptide chain can be digested into stable fragments, providing an opportunity to obtain novel information about the folding units of a protein.

Horse heart cytochrome *c* (cyt *c*) is a single-chain hemoprotein of 104 amino acid residues, with a structure composed of three major and two minor α-helices. The prosthetic group is covalently bound by two thioether bridges to two cysteine residues, Cys14 and Cys17. Under physiological conditions, His18 and Met80 are the axial ligands of the heme iron. Met80 is thought to play a significant functional role for the protein, being considered the residue responsible for the relatively high redox potential of cyt *c* [7].

Kinetic and equilibrium intermediates of cyt *c* have been characterized by a variety of techniques, such as stopped-flow [8, 9, 10, 11, 12, 13], nuclear magnetic resonance [14, 15], resonance Raman [16, 17, 18], and circular dichroism [19, 20, 21] spectroscopies. In recent years, several authors have investigated the properties of cyt *c* reconstituted from fragments of different length (see, for example, [22, 23, 24, 25, 26] and references therein). More recently, we reported the properties of

the residues 1–56 heme-containing fragment of horse cyt *c* obtained by limited proteolysis of the parent protein [27, 28], and of the non-covalent fragment complex obtained from the combination of the two contiguous (residues 1–56 heme-containing and residues 57–104) fragments [29].

The present paper reports an investigation of the structural and redox properties of the non-covalent complex reconstituted upon mixing the residues 1–38 heme-containing N-fragment with the residues 57–104 C-fragment of the protein (see Fig. 1). With respect to native cyt *c*, the complex lacks a segment of 18 residues corresponding, in the native protein, to an omega (Ω)-loop region [30]. Ω-Loops have been indicated as a discrete category of protein secondary structure, characterized by a random coil conformation and by a necking of the two termini [31]. Moreover, they have been proposed to play a role in protein folding and functionality. In native cyt *c*, the 40s Ω-loop is constituted by residues 40–57; the segment terminal residues (40 NH, 57 CO) are H-bonded and the loop is stabilized by 32 intraloop side-chain contacts. As revealed by X-ray crystallography [30], the H-bond between the imidazole group of His26 and the backbone carbonyl of Pro44 bridges the 20s and the 40s Ω-loops in the polypeptide chain. This stabilizes the protein tertiary conformation and favors the shielding action of the 40s loop on the bottom heme edge. Thus, the 40s Ω-loop is critical for the structural and functional properties of the protein. This loop is the least conserved in the protein evolution, and class I cytochromes have been classified on the basis of its presence (or absence) [32]. Further, this loop seems to play a role in cyt *c* binding to lipid membranes and in the alkaline transition [33, 34, 35]. Excision of the 40s Ω-loop in horse cyt *c* [23] gives rise to a protein which is structurally similar to cyt c_{555} of the green sulfur bacterium *Chlorobium thiosolfatophilum*, which has a redox potential, $E^\circ = 145$ mV vs. NHE, significantly lower than that ($E^\circ = 250$ mV) of horse cyt *c* [36]. The present study of the residues 1–38/57–104 fragment complex aims to provide novel information on the role played by the 40s Ω-loop in cyt *c*.

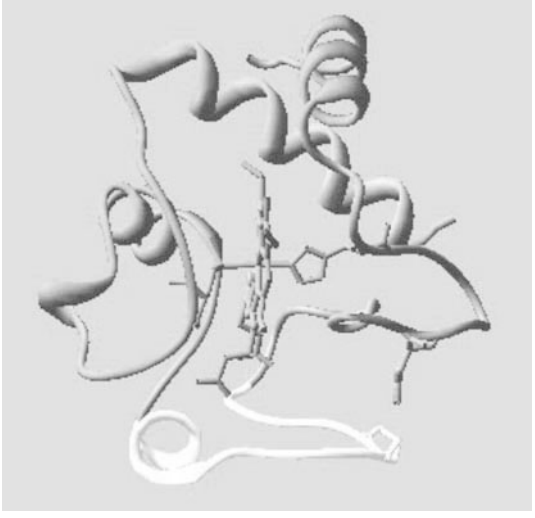

Fig. 1 Ribbon structure of horse cyt *c*. The excised Ω-loop is shown in *white*. The heme group with the heme axial ligands (His18, *right*; Met80, *left*) and (*bottom right*) residues His26 (*gray*) and Pro44 (*white*) are represented as *sticks*. The protein structure [30] was visualized with the Swiss-Pdb Viewer software [62]

Materials and methods

Materials

Horse heart cyt *c* (type VI) and thermolysin were purchased from Sigma (St. Louis, Mo., USA) and used without further purification. Clostripain was obtained from Worthington (Lakewood, NJ, USA). High-purity guanidine (Gdm-HCl) was obtained from ICN (Costa Mesa, Calif., USA). 4,4′-Bipyridine was obtained from Merck (Darmstadt, Germany). All the reagents used were of analytical grade.

Fragmentation of cyt *c*

Residues 57–104 fragment

Digestion of cyt *c* was performed as previously described [27, 29]. Briefly, the protein (1 mg/mL) was dissolved in 20 mM Tris-HCl buffer (pH 7.8) containing 10 mM $CaCl_2$ and incubated with thermolysin (protein substrate:protease ratio, 50:1 by mass) at 25 °C for 24 h, in the presence of 50% trifluoroethanol.

Residues 1–38 fragment

Cyt *c* (1 mg) dissolved in 20 mM Tris-HCl buffer (pH 7.8) containing 10 mM $CaCl_2$ was incubated for 24 h (at 37 °C) with 50 μL of previously activated clostripain, in the presence of 50% trifluoroethanol. Activation of the protease was achieved by incubating for 3 h (at room temperature) 4 U of clostripain dissolved in 50 μL of 10 mM Tris-HCl buffer (pH 7.8) containing (1) 50 mM $CaCl_2$, (2) 160 mM NaCl, (3) 2.5 mM DTT.

For both fragments, the digestion mixtures were analyzed by SDS-PAGE and the proteolysis products identified by the N-terminal amino acid sequence. Fragments were purified by reverse-phase HPLC using a Vydac C4 column and their identities confirmed by electrospray ion (ESI) mass spectrometry. Concentrations of the two fragments were determined by considering a value of $\epsilon_{408} = 118\ mM^{-1}\ cm^{-1}$ for the heme-containing residues 1–38 (or N-) fragment and a value of $\epsilon_{280} = 12\ mM^{-1}\ cm^{-1}$ for the residues 57–104 (or C-) fragment [29].

Circular dichroism measurements

CD measurements were carried out using a Jasco J-710 spectropolarimeter (Tokyo, Japan) equipped with a PC as data processor. The molar ellipticity, $[\theta]$ (deg cm^2 $dmol^{-1}$), is expressed on a molar heme basis in the Soret (380–450 nm) region and as mean residue ellipticity in the far-UV region (200–250 nm, mean residue molecular mass = 119). Experiments were performed at neutral pH, in 0.1 M phosphate buffer.

Formation of the ferric fragment complex was followed in the far-UV region by recording the increase of the negative Cotton effect at 222 nm (indicative of recovery of the α-helix conformation) upon stepwise addition of the C-fragment to a solution of the heme-containing N-fragment. Substoichiometric amounts of a concentrated C-fragment solution (60 μM) were added, at 25 °C, to a 6 μM N-fragment solution (0.1 M phosphate buffer, pH 7.0) and the dichroic spectrum recorded. The maximum increase in ellipticity was observed at a 1:1 molar ratio (see Results section); subsequently the CD signal remained constant, even after addition of a significant excess of the C-fragment (2:1 molar ratio).

Electronic absorption measurements

Electronic absorption measurements were carried out at 25 °C using a Cary 5 spectrophotometer. The extinction coefficients $\epsilon_{408} = 106$ (cyt *c*) and $\epsilon_{406} = 106$ mM^{-1} cm^{-1} (both the residues 1–38/57–104 and the residues 1–56/57–104 fragment complexes) were used to determine sample concentrations. Sample concentrations for both the absorption and resonance Raman (RR) spectra were in the range 35–80 μM. A very small amount of potassium hexacyanoferrate(III) (2–8 μM) was added to the solution of the cyt *c* and His26Tyr mutant samples to ensure that they were completely oxidized. For both absorption and RR samples the following buffers were used: 0.1 M sodium phosphate at pH 5.0 and 7.0; 0.1 M borate at pH 9.6.

Resonance Raman measurements

RR spectra were obtained at room temperature with excitation from the 406.7 nm line of a Kr^+ laser (Coherent, Innova 302). The back-scattered light from a slowly rotating NMR tube was collected and focused into a computer-controlled double monochromator (Jobin-Yvon HG2S) equipped with a cooled photomultiplier (RCA C31034A) and photon counting electronics. To minimize local heating of the protein by the laser beam, the sample was cooled by a gentle flow of N_2 gas passed through liquid N_2. RR spectra were calibrated to an accuracy of 1 cm^{-1} for intense isolated bands, with indene as the standard for the high-frequency region and with indene and CCl_4 for the low-frequency region.

Direct current cyclic voltammetry measurements

Voltammetric measurements were carried out at 25 °C in a glass microcell (sample volume: 1 mL) equipped with a reference calomel electrode (Amel, Milan, Italy), a Pt wire as the counter electrode and a gold electrode (2 mm diameter, Amel) with adsorbed 4,4′-bipyridine [37] as the working electrode.

An Amel 433/W multipolarograph (Milan, Italy), interfaced with a PC, was employed for voltammetric measurements. Before the voltammetric experiment, the solution containing 0.10 mM complex and 10 mM 4,4′-bipyridine was deaerated for 30 min by a gentle flow of pure N_2 maintained just above the solution surface.

Catalytic activity measurements

Polarographic measurements were carried out at room temperature using a Clark-type O_2 electrode (Ysi model 5300, Yellow Spring, Ohio, USA) interfaced with a recorder. The oxygen probe was inserted into a 0.6 mL chamber (Instech Laboratories, model 600A, Horsham, Pa. USA) containing 57 nM bovine cyt *c* oxidase dissolved in 50 mM phosphate buffer, pH 7.0, in the presence of 10 mM ascorbate and 0.23 mM *N*,*N*,*N*′,*N*′-tetramethyl-*p*-phenylenediamine (TMPD). Increasing amounts of cyt *c* or of the fragment complex were then added, and slope changes recorded. Catalytic activities were calculated as turnover numbers, from the rates corrected for the non-enzymatic oxygen consumption.

Results

The residues 1–38 heme-containing fragment

The electronic absorption and RR spectra of the ferric (residues 1–38) fragment are very similar to those of the residues 1–56 fragment [27, 28], suggesting closely similar structural features. In particular, the absorption spectrum of the residues 1–38 fragment at pH 7.0 (Soret band at 407 nm, Q bands at 528 and 555 nm) is identical to that of the residues 1–56 fragment, except for a 1 nm red shift of the Soret band (Table 1). The high-frequency RR spectra of both fragments at pH 7.0 are upshifted by ca. 3 cm^{-1} compared to the native protein (residues 1–38 fragment: $\nu_3 = 1506$, $\nu_2 = 1588$, $\nu_{10} = 1640$ cm^{-1}; residues 1–56 fragment: $\nu_3 = 1505$, $\nu_2 = 1587$, $\nu_{10} = 1639$ cm^{-1}; Table 1 [28]). The pronounced saddling distortion of the heme group in the native structure [38] is manifested in the RR spectra by the lower frequencies of the core size marker bands compared to planar heme proteins, which display an inverse correlation between the RR band frequencies and the metalloporphyrin core size [39, 40, 41, 42]. Therefore, the spectral features of the two fragments are characteristic of a less distorted heme, are typical of a bis-His low-spin heme coordination [28, 43], and confirm their structural similarity. Figure 2

Table 1 Electronic absorption and RR parameters of the cyt *c* fragments and fragment complexes[a]

	Soret (nm)	Q bands (nm)		RR bands (cm^{-1})		
				ν_3	ν_2	ν_{10}
Horse cyt *c*, pH 7[b]	409	530	555	1502	1584	1635
Horse cyt *c*, pH 9.6	406	530	555	1504[c]	1585[c]	1636[c]
Residues 1–38 fragment, pH 7	407	528	555	1506	1588	1640
Residues 1–56 fragment, pH 7[d]	406	528	555	1505	1587	1639
Residues 1–38/57–104 complex, pH 5	408	528	555	1504	1585	1637
Residues 1–38/57–104 complex, pH 7	407	528	555	1504	1586	1637
Residues 1–38/57–104 complex, pH 9	407	528	555			
Residues 1–56/57–104 complex, pH 5	408	529	555	1504	1585	1637
Residues 1–56/57–104 complex, pH 7	407	528	555	1504	1586	1637
Residues 1–56/57–104 complex, pH 9	407	528	555			

[a]Measured in this work unless otherwise noted
[b]From [16, 17, 43]
[c]See also [44]
[d]From [28]

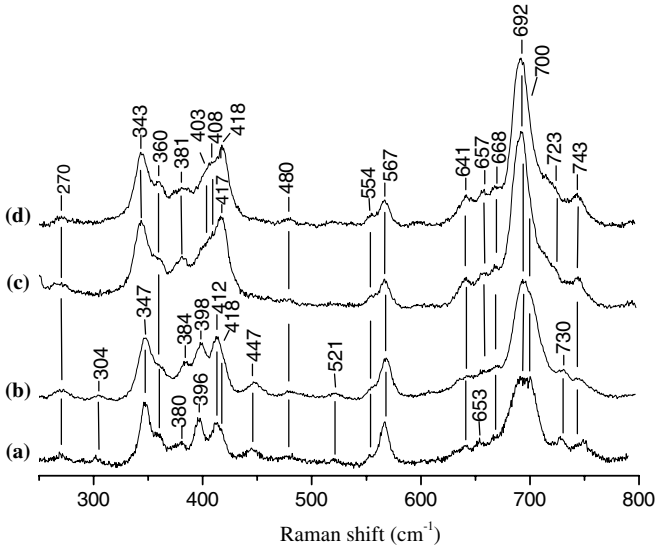

Fig. 2 Low-frequency RR spectra of cyt *c* at pH 7.0 (*a*) and 9.6 (*b*), the residues 1–56 fragment at pH 7.0 (*c*) and the residues 1–38 fragment at pH 7.0 (*d*). Experimental conditions: 406.7 nm excitation, 5 cm^{-1} resolution; (*a*) 15 mW laser power at the sample, 3 s/0.5 cm^{-1} collection interval; (*b*) 10 mW laser power at the sample, 11 s/0.5 cm^{-1} collection interval; (*c*) 20 mW laser power at the sample, 8 s/0.5 cm^{-1} collection interval; (*d*) 10 mW laser power at the sample, 14 s/0.5 cm^{-1} collection interval

compares the low-frequency RR spectra of the two fragments at pH 7.0 with those of the native protein at neutral and alkaline pH. Since the low-frequency RR spectrum is very sensitive to variations in heme distortion [44], the close resemblance of the spectra of the two fragments underlines that their fine structural details are essentially identical. Moreover, the four spectra display differences in both band frequencies and intensities, particularly in the region 340–420 cm^{-1}. The heme of cyt *c* has a pronounced distortion due to interaction with the protein matrix through thioether links between the heme and two cysteine residues [30, 44, 45]. The heme distortion leads to a very rich low-frequency RR spectrum as out-of-plane modes become active. The change of axial coordination from Met to His (in the fragments) or Lys (in cyt *c* at pH 9.6 [44]) leads to a reduction of the heme distortion and causes an intensity decrease of the out-of-plane modes γ_{22}, γ_2 and γ_5 at 447, 567 and 730 cm^{-1}, respectively, and a frequency downshift of the ν_7 mode (700 cm^{-1}) [16, 28, 34, 43, 46, 47]. The downshift of the latter mode and resultant better overlap with the ν(C–S) mode (692 cm^{-1}) leads to a sharpening of the overall band. Therefore, the low-frequency region may provide a clear means of distinguishing between low-spin heme species in which the sixth ligand is a Met (cyt *c*, pH 7.0, Fig. 2, spectrum a), Lys (cyt *c* at pH 9.6, spectrum b) or His (fragments at pH 7.0, spectra c and d) residue.

The redox potential of the residues 1–38 fragment determined by CV at pH 7.0, $E^\circ = 57 \pm 7$ mV vs. NHE, is lower than that of the parent protein (250 mV), but significantly higher than that of free heme ($E^\circ = -120$ mV vs. NHE) [48] and microperoxidase ($E^\circ = -160$ mV vs. NHE) [49]. As for the case of the residues 1–56 fragment ($E^\circ = 0$ mV [27]), it falls in the redox potential range observed for bis-His coordinated systems [50, 51], consistent with the bis-His character of the fragment and some shielding action exerted on the heme by the peptide.

The ferric (residues 1–38/57–104) fragment complex

Circular dichroism

The reconstitution reaction of the ferric (residues 1–38/57–104) fragment complex was followed by CD in the far-UV region (200–250 nm), as reported earlier [29]. Briefly, formation of α-helix structure (see the Materials and methods section for details) was monitored by stepwise addition of submolar amounts of the C-fragment to the N-fragment (taken singly, both the C- and the N-fragments are unstructured in solution). The

titration curve obtained from ellipticity values at 222 nm, shown in Fig. 3, indicates that at a molar ratio of 1:1 the two fragments give rise to a complex with native-like α-helix structure. In fact, the α-helix content (approx. 29%) determined for the fragment complex is very close to that shown by the intact protein (approx. 32%). Figure 4 shows the Soret (400–450 nm) CD spectrum of the complex recorded at 5 °C and 25 °C. It is evident that the 416-nm dichroic band of the complex, which is considered diagnostic for the Met80–Fe(III) axial bond in native cyt *c* [52, 53], is weaker than that of the intact protein and is temperature dependent (see Table 2). In accord with a recent report [34], the weak 416-nm signal may be indicative for some heterogeneity in solution. It is noted that the Met–Fe(III)–His

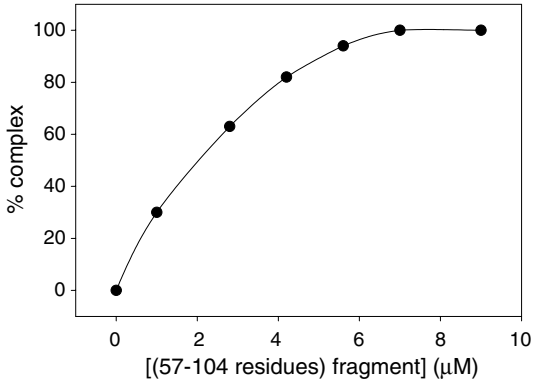

Fig. 3 Titration curve of the residues 1–38 heme-containing fragment (6 μM) with increasing amounts of the residues 57–104 fragment, as obtained from CD data at 222 nm. Experimental conditions: 0.1 M phosphate buffer, pH 7.0

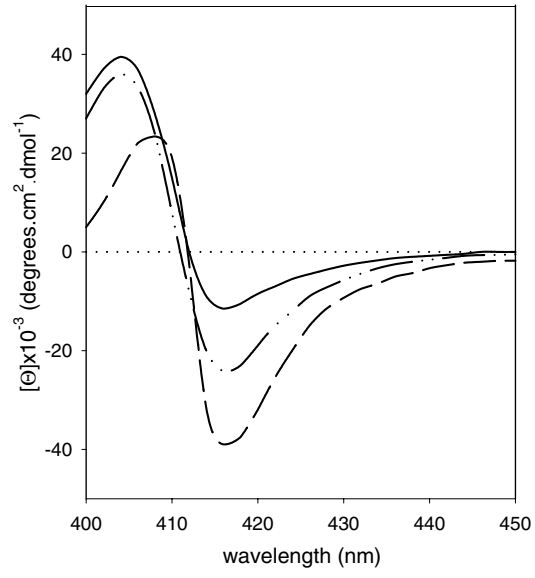

Fig. 4 Soret CD spectrum of the residues 1–38/57–104 fragment complex from horse cyt *c* at 5 °C (*dot-dashed line*) and 25 °C (*solid line*). Experimental conditions: 0.1 M phosphate buffer, pH 7.0. The spectrum of the intact protein (*dashed line*) is shown for comparison

Table 2 Molar ellipticity values of the 416-nm Cotton effect and p *K* values of the alkaline transition

	$[\Theta]_{416}$ (25 °C)	$[\Theta]_{416}$ (5 °C)	p K_{695}[a] (25 °C)
Residues 1–38/57–104 complex	−11,500	−24,000	
Low-pH state transition			6.72 (±0.06)
High-pH state transition			8.56 (±0.06)
Residues 1–56/57–104 complex	−22,600[b]	−39,500[b]	7.08 (±0.08)
Horse cyt *c*	−39,500[b]	−39,500[b]	8.90 (±0.06)[c]

[a]Determined from the absorbance change at 695 nm
[b]From [29][c]From [54]

coordinated species alone contributes to the signal at this wavelength; an equilibrium between (at least) two species, Met80–Fe(III)–His18X–Fe–His18 (where X is an endogeneous ligand misligated to the metal) is therefore expected. The 416-nm Cotton effect is reversibly influenced by temperature in the range 5–25 °C; the stronger signal at low temperature suggests stabilization of the native Met-His coordination upon lowering the temperature.

Electronic absorption and resonance Raman

Figure 5 shows the absorption spectra of the ferric (residues 1–38/57–104) fragment complex at pH 7.0 and 5.0. At pH 7.0 (Fig. 5c) the spectrum is blue shifted compared to cyt *c* (Fig. 5a) and the charge transfer band at 695 nm {considered diagnostic for the Met80–Fe(III) axial bond in the native protein [55]} is weaker. In accord with the CD results, these data indicate the presence of a misligated species in equilibrium with the

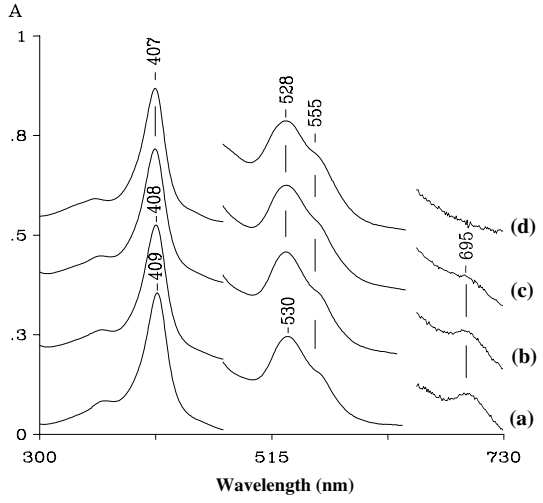

Fig. 5 Electronic absorption spectra at 25 °C of cyt *c* at pH 7.0 (*a*), the residues 1–38/57–104 fragment complex at pH 5.0 (*b*) and pH 7.0 (*c*), and the residues 1–38 fragment at pH 7 (*d*). The spectral regions between 470–650 and 650–730 nm are expanded 6- and 60-fold, respectively. The path length of the cuvette was 1 mm for all spectra. The ordinate scale refers to spectrum (*a*)

native cyt *c* Met80–Fe(III)–His18 axial coordination. In fact, apart from the weak band at 695 nm, the spectrum closely resembles that of the residues 1–38 fragment at pH 7.0 (Fig. 5d), which is a bis-His coordinated low-spin heme. At pH 5.0 (Fig. 5b) the Soret band of the fragment complex is red shifted by 1 nm compared to pH 7.0 and the 695 nm band is more intense, indicating a decreased amount of misligated species at this pH.

The absorption spectrum of the fragment complex at pH 9.0 is essentially identical to that at pH 7.0, except for the complete absence of the 695 nm band, and similar to that of native cyt *c* at alkaline pH (Table 1). The residues 1–56/57–104 fragment complex displays similar behavior (see Table 1).

The frequencies of the core size marker bands in the high-frequency region of the RR spectrum of the ferric (residues 1–38/57–104) fragment complex at pH 7.0 are slightly upshifted ($\nu_3 = 1504$, $\nu_2 = 1586$, $\nu_{10} = 1637$ cm^{-1}) compared to the native protein (Table 1). At pH 5.0 the spectrum remains essentially unchanged. The spectrum is also very similar to that of the residues 1–56/57–104 fragment complex at pH 7.0 and 5.0 (Table 1). As discussed above, the upshift of the RR frequencies is indicative of a relaxation of the heme distortion following a change of axial heme coordination to either a histidine or lysine residue. Hence, both the electronic absorption and high-frequency RR spectra, in agreement with the CD data, reveal the presence of a misligated species in the residues 1–38/57–104 fragment complex which appears to decrease upon lowering the pH from 7.0 to 5.0, but they are unable to determine whether the misligated ligand is a histidine or lysine residue. However, as noted before, the low-frequency RR spectrum region between 340–420 cm^{-1} can provide a clear means of distinguishing between hexacoordinate low-spin heme species in which the sixth ligand is a His or Lys residue. Figure 6 shows the low-frequency RR spectra of the residues 1–38/57–104 (a) and 1–56/57–104 (b) fragment complexes at pH 7.0 (dotted lines) and 5.0 (continuous lines). The corresponding spectra of the His26Tyr mutant of iso-1-cyt *c* (c) are also reported for comparison since we recently showed that the alkaline conformer of cyt *c* is populated at pH 7.0 in this mutant and the sixth ligand of the misligated species was proposed to be a lysine [33]. Upon decreasing the pH from 7.0 to 5.0 the misligated ligand, particularly if lysine, is expected to become protonated. Therefore, the misligated species is likely to decrease sufficiently to lead to an increase of the native form and, consequently, a modified RR spectrum is expected. A number of changes are evident in the low-frequency RR spectrum of the residues 1–38/57–104 fragment complex upon decreasing the pH from 7.0 to 5.0. In particular, modes involving the thioether bridges and the ν_8 mode are affected. There is an overall 2 cm^{-1} downshift of the $\delta(C_\beta C_a S)$ band at 399 cm^{-1}, the $\delta(C_\beta C_a C_b)$ band at 413 cm^{-1} decreases markedly and the ν_8 mode at 347 cm^{-1} sharpens and shifts 2 cm^{-1} to high frequency. Similar changes with pH are observed for the residues 1–56/57–104 fragment

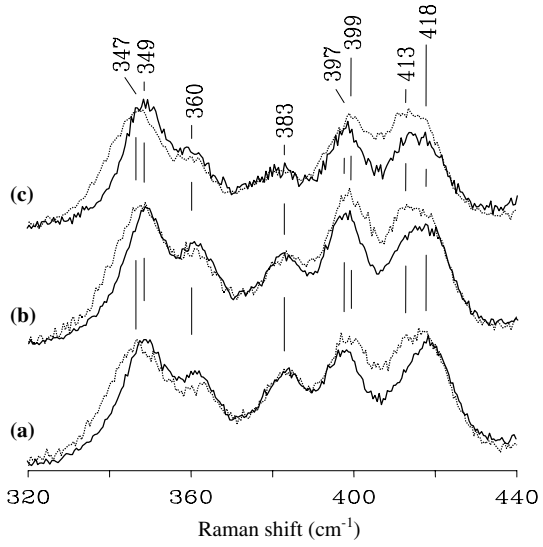

Fig. 6 Low-frequency RR spectra at pH 5.0 (*solid line*) and pH 7.0 (*dotted line*) of the residues 1–38/57–104 fragment complex (*a*), the residues 1–56/57–104 fragment complex (*b*) and the H26Y mutant of iso-1-cyt *c* (*c*). Experimental conditions: 406.7 nm excitation, 5 cm^{-1} resolution, 10 mW laser power at the sample; (*a*, pH 5.0) 13 s/0.5 cm^{-1} collection interval; (*a*, pH 7.0) 12 s/0.5 cm^{-1} collection interval; (*b*, pH 5.0) 13 s/0.5 cm^{-1} collection interval; (*b*, pH 7.0) 7 s/0.5 cm^{-1} collection interval; (*c*, pH 5.0) 6 s/0.5 cm^{-1} collection interval; (*c*, pH 7.0) 8 s/0.5 cm^{-1} collection interval

complex and for the His26Tyr mutant of iso-1-cyt *c*. The latter is an equilibrium of two species at pH 7.0, one having native Met80–Fe(III)–His18 coordination and the other a misligated Lys–Fe(III)–His18 coordination [34]. These observations are consistent with changes that follow the alkaline transition of cyt *c* ([44]; Fig. 2, spectrum b), which prompts the replacement of Met80 by two lysine residues (Lys73 and Lys79) [44]. Furthermore, they are not consistent with the changes that would be expected for a misligated species involving a bis-His heme coordination. In this case, upon decreasing the pH the band at 418 cm^{-1} would be expected to decrease in intensity whereas the intensity of the bands at 413 and 399 cm^{-1} should increase (Fig. 2; [28]). Hence, the low-frequency RR spectra favor a lysine rather than histidine residue as the misligated ligand in the residues 1–38/57–104 fragment complex.

Alkaline transition

The alkaline titration of the residues 1–38/57–104 fragment complex was investigated by following the change of the absorption band at 695 nm in the pH range 6.0–9.0. In cyt *c*, this event induces a tertiary rearrangement of the protein, coupled to the replacement of Met80 by a lysine at the sixth coordination position of the heme-iron [54, 55]. The alkaline transition of the residues 1–38/57–104 fragment complex is very different from that of the native protein, displaying a peculiar biphasic behavior. From the transition profile, shown in Fig. 7, a low and a high

pK_a-associated state transition can be distinguished. The former does not fully eliminate the 695 nm absorbance, while in the latter the signal is totally lost. The transition proved to be fully reversible. The alkaline titration of the residues 1–56/57–104 fragment complex, whose profile is shown in the same figure, displays instead a monophasic behavior, although the transition occurs at a pH lower than that of the native protein (the pK_a values of the alkaline transitions are reported in Table 2).

Denaturation studies

The unfolding titration of the ferric fragment complex, induced at neutral pH by increasing amounts of Gdm-HCl, was investigated by CD at both 222 nm and 408 nm, to probe both the α-helix structure and the heme pocket conformation, respectively. All the points followed the same titration profile, indicating that the secondary and tertiary structures of the complex unfold simultaneously. The unfolding profile (not shown) closely resembles that of the residues 1–56/57–104 complex [29]. Thermodynamic parameters for the Gdm-HCl denaturation of the fragment complex are reported in Table 3. The value of the denaturant concentration at the transition midpoint, $C_{1/2}$, and that of the apparent free energy change, ΔG_D [obtained from the apparent denaturation equilibrium constant, K_D, determined from the expression $K_D = (\theta_i - \theta_{obs})/(\theta_{obs} - \theta_f)$, where θ_i, θ_f and θ_{obs} represent the initial, final and observed values of ellipticity, respectively] are lower than the respective parameters of the native protein, in agreement with a reduced complex stability. The apparent free energy change in the absence of denaturant, ΔG_0, was estimated on the assumption of a linear dependence of ΔG_D versus denaturant concentration [56]. The value obtained, $\Delta G_0 = 13.9 \pm 1.2$ kJ/mol, is close to that determined for the residues 1–56/57–104 complex [24], and approximately one half that of the native protein. The value of m, a parameter that measures the dependence of ΔG_D on the denaturant concentration [D] (according to the empirical equation $\Delta G_D = \Delta G_0 - m[D]$), is within the error, slightly lower than that of the native protein (see Table 3). Since m is assumed to be proportional to the change of the solvent-accessible area of a protein upon unfolding [56, 57], this suggests a slightly reduced compactness of the complex.

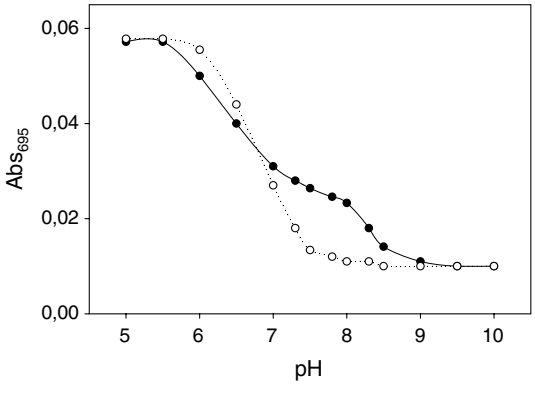

Fig. 7 Plots of A_{695} versus pH for the residues 1–38/57–104 (*solid circles*) and residues 1–56/57–104 (*open circles*) fragment complexes. Experimental conditions: 0.1 M phosphate buffer and 25 °C; complex concentrations were about 100 μM. The pH of the sample (V_i: 2.0 mL) was varied by adding a few μL of 0.5 M NaOH or HCl solution, until the desired pH was reached. The absorbance recorded was always corrected for the dilution factor

Table 3 Thermodynamic parameters for Gdm-HCl-induced denaturation[a]

	$C_{1/2}$ (M)	ΔG_0 (kJ/mol)	m [(kJ/mol)/M]
Residues 1–38/57–104 complex	1.35 (±0.06)	13.5 (±1.6)	10.0 (±1.8)
Residues 1–56/57–104 complex	1.34[b]	15.7[b]	12.0[b]
Horse cyt *c*	2.42[c]	30.4[c]	12.5[c]

[a]Experimental conditions: 0.1 M phosphate buffer, pH 7.0, and 25 °C
[b]From [29]
[c]From [56]

Redox properties

At pH 7.0 and 25 °C the cyclic voltammograms of the residues 1–38/57–104 fragment complex exhibit a defined electrochemistry at scan rates ranging between 20 and 200 mV/s (data not shown). The redox potential, $E_{1/2} = 191 + 6$ mV vs. NHE, is lower than that of the native protein (250 mV [20]), but high enough to suggest that the native Met80–heme-iron axial bond is recovered. In fact, a considerable decrease of the redox potential is observed when the methionine of cyt *c* is replaced by another side chain at the axial position [50, 51, 58], even if the heme remains efficiently shielded by the peptide chain. The 59 mV drop with respect to the redox potential of the intact protein can be ascribed, at least in part, to removal of the residues 39–56 segment, that renders more open and solvent-accessible the tertiary conformation of the complex.

Figure 8 shows the redox reaction between the residues 1–38/57–104 fragment complex (in the reduced state) and cyt *c* oxidase, the biological reaction partner of cyt *c*. It is clearly evident that the catalytic activity typical of the protein is fully retained by the fragment complex, indicating that interaction with cyt *c* oxidase is unaffected by removal of the 40s Ω-loop. Conversely, the heme-containing residues 1–38 N-fragment shows no reaction with cyt *c* oxidase (Fig. 8), which excludes complex dissociation into the fragments during the electron-transfer reaction.

Discussion

Over recent years, reports dealing with the properties of fragment complexes derived from cyt *c* have significantly

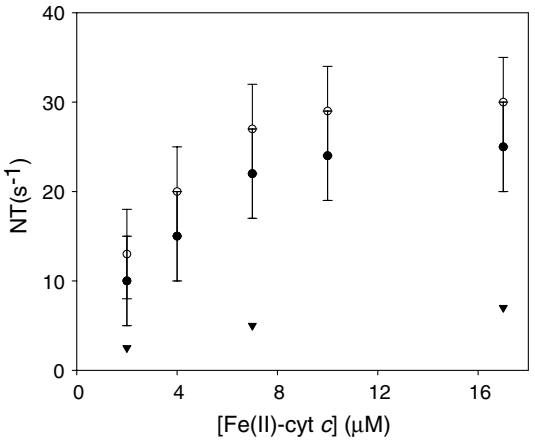

Fig. 8 Catalytic activity, calculated as turnover numbers, of reconstituted fragments (*open circles*) and native (*solid circles*) Fe(II)-cyt *c* with cyt *c* oxidase (for details, see text). The behavior of the heme-containing residues 1–38 fragment (*inverted triangles*) is shown for comparative purposes. Experimental conditions: 0.1 M phosphate buffer, pH 7.0, containing 57 nM bovine cyt *c* oxidase plus 10 mM ascorbate and 0.23 mM TMPD as reductants

contributed to a better understanding of the properties of macromolecules formed by the non-covalent interaction between two peptides. Fragment complexes often show a compact structure and retain, at least in part, the biological functionality of the parent protein. As compact states of proteins, fragment complexes may provide valuable insight into aspects of protein folding, as they can represent stable models of kinetic intermediates which form during the folding process.

Recently, we reported the properties of a non-covalent complex of horse cyt *c* formed by two contiguous fragments, namely the residues 1–56 heme-peptide and the residues 57–104 peptide [29]. This complex lacks the peptide bond between Gly56 and Ile57 located, in the intact protein, at one end of the 40s Ω-loop (see Fig. 1). It is characterized by a native-like α-helix structure, a compact non-native tertiary conformation, and a redox potential close to that of the intact protein. Further, it shows catalytic activity in the reaction with cyt *c* oxidase.

The non-covalent fragment complex investigated here is formed by two non-complementary fragments, namely the residues 1–38 heme-peptide and the residues 57–104 peptide. The absence of the segment of 18 residues corresponding to the 40s Ω-loop [30] (see Fig. 1) allows us to gain novel information on the role played by this loop in protein structure, stability and functionality. As found for the residues 1–56/57–104 complex, at pH 7.0 the residues 1–38/57–104 fragment complex shows native-like α-helix structure and appreciable compactness, indicating that the excision of the 40s Ω-loop causes some structural alteration. However, this is much less extensive than that observed in the completely unfolded macromolecule. In comparison with the intact protein, the complex shows a flexible tertiary structure with altered heme pocket conformation and weakened Met80–Fe(III) axial bond strength. As the spectroscopic data clearly show, at neutral pH the complex cannot be treated as a single species system. At least two distinct conformers are observed in solution, one with native Met–Fe(III)–His coordination, the other, L–Fe(III)–His, with a nonnative axial ligand (L = His or Lys residue) coordinated to the heme-iron(III) in place of Met80.

In this regard, it is noteworthy that the residues 1–38/57–104 fragment complex has a biphasic alkaline titration (Fig. 7) characterized by a low ($pK_{a1} = 6.72$) and a high ($pK_{a2} = 8.56$) pK_a-associated state transition. This behavior differs from that of both native cyt *c* and the residues 1–56/57–104 fragment complex. In fact, although the latter two systems have different pK_a values, both show monophasic transitions (Table 2). The pK_{a2} of the residues 1–38/57–104 fragment complex is close to that determined for the alkaline transition of native cyt *c* ($pK_a = 8.9$ [54]), suggesting that a lysine side chain (either Lys73 or Lys79, as for the alkaline form of native cyt *c* [44]), displaces the native Met80 [55, 59]. The nature of the ligand (L_1) responsible for the pK_{a1} cannot be immediately identified. Although pK_{a1} falls in a range of values typical of histidine residues, it is also compatible with that of a buried lysine which is characterized by a depressed pK_a (about 6.0) [60].

A recent paper has reported a biphasic alkaline transition for the Lys73His variant of iso-1-cyt *c* [59]. Its pK_{a1} value (6.7 ± 0.1), ascribed to His73, is very close to that presently found for the residues 1–38/57–104 fragment complex. However, since in that study mutation occurs in the Met80-containing loop, binding of His73 to the metal in place of Met80 is not expected to be coupled with large changes in the tertiary conformation of the protein. On the contrary, the histidines that in principle can axially coordinate to the iron(III) in the residues 1–38/57–104 fragment complex are His26 and His33, which are located on the opposite side of the macromolecule with respect to the Met80-containing loop (Fig. 1). Therefore, axial binding of one of these two histidines to the metal is expected to induce large tertiary changes in the protein that would significantly affect protein stability. Such behavior is not found for either the residues 1–38/57–104 or the residues 1–56/57–104 complex. Moreover, the low-frequency RR spectra clearly favor a lysine rather than histidine residue as the misligated L_1 ligand. This conclusion is also consistent with the closely similar values of the pK_a and the denaturation free energy (ΔG_D) values for the alkaline transition of the residues 1–38/57–104 complex and the H26Y variant of yeast iso-1-cyt *c* (6.72 vs. 7.48, and 13.5 vs. 14.8 kJ/mol, respectively). The residue considered responsible for displacement of Met80 in the latter case is a lysine located in the Met80-containing loop [34]. However, on the basis of the presently available data, it is not possible to identify which of the three possible lysine ligands (Lys72, Lys73, Lys79) is actually bound to the heme iron.

From a functional point of view, the catalytic activity of the residues 1–38/57–104 fragment complex with cyt *c*

oxidase at neutral pH is comparable to that of native cyt *c*. This excludes fragment dissociation upon reduction (the residues 1–38 heme-containing fragment shows no catalytic activity) and provides further support for the considerations made above concerning the nature of L_1. The catalytic activity exhibited by the complex renders unlikely the hypothesis that His26 and/or His33 bind to the heme-iron(III) in place of Met80, since this would cause a large tertiary rearrangement.

The redox potential determined for the residues 1–38/57–104 fragment complex is lower than that of the intact protein ($\Delta E^{\circ} = 59$ mV), suggesting that the heme is less solvent-shielded by the polypeptide (which is not surprising, given the absence of a 18-residues loop region), but still buried within the protein matrix. Interestingly, the redox potential of the complex falls within a redox potential range common to several other two-fragment complexes having the cleavage site in the 40s Ω-loop [61]. This underlines the important role of the 40s Ω-loop for the stabilization of the native conformer and for strengthening the Met80–Fe(III) coordination bond, as clearly revealed by our spectroscopic data.

In conclusion, the results obtained for the residues 1–38/57–104 fragment complex highlight the role played by the 40s Ω-loop for stability of cyt *c*. As here shown, the excision of the loop destabilizes the protein, lowers the pK_a of the alkaline transition, and renders the transition biphasic. This last point is of particular interest as several authors have proposed the alkaline conformer to be a heterogeneous biosystem [54]. If so, the excision of the residues 39–56 loop enhances the difference of affinity for the heme-iron(III) of one component with respect to the other(s).

Acknowledgements The authors wish to thank P. Sarti and E. Forte (Dipartimento di Biochimica, Università di Roma "La Sapienza") for assistance in the polarographic measurements, and E. Schininà (Dipartimento di Biochimica, Università di Roma "La Sapienza") for mass spectrometric measurements. This research was funded in part by grants from the Italian MIUR (COFIN 2001 031798).

References

1. Kuwajima K (1989) Proteins 6:87–103
2. Creighton TE (1990) Biochem J 270:1–15
3. Kim PS, Baldwin RL (1990) Annu Rev Biochem 59:631–660
4. Ptitsyn OB (1992) In: Creighton TE (ed) Protein folding. Freeman, New York, pp 243–300
5. Privalov PL (1996) J Mol Biol 258:707–725
6. Fontana A, Zambonin M, De Filippis V, Bosco M, Polverino de Laureto P (1995) FEBS Lett 362:266–270
7. Moore GR, Pettigrew GW (1990) Cytochromes c. Evolutionary, structural and physiological aspects. Springer, Berlin Heidelberg New York
8. Sosnick TR, Mayne L, Hiller R, Englander SW (1994) Nat Struct Biol 1:149–156
9. Colón W, Roder H (1996) Nat Struct Biol 3:1019–1025
10. Takahashi S, Yeh S-R, Das TK, Chan C-K, Gottfried DS, Rousseau DL (1997) Nat Struct Biol 4:44–50
11. Yeh, S-R, Takahashi S, Fan B, Rousseau DL (1997) Nat Struct Biol 4:51–56
12. Bai Y (1999) Proc Natl Acad Sci USA 96:477–480
13. Pierce MM, Nall BT (2000) J Mol Biol 298:955–969
14. Jeng MF, Englander SW (1991) J Mol Biol 221:1045–1061
15. Russell BS, Melenkivitz R, Bren K (2000) Proc Natl Acad Sci USA 97:8312–8317
16. Jordan T, Eads JC, Spiro TG (1995) Protein Sci 4:716–728
17. Oellerich S, Wackerbarth H, Hildebrandt P (2002) J Phys Chem B 106:6566–6580
18. Sinibaldi F, Howes BD, Smulevich G, Ciaccio C, Coletta M, Santucci R (2003) J Biol Inorg Chem 8:663–670
19. Goto Y, Takahashi N, Fink AL (1990) Biochemistry 29:3480–3488
20. Marmorino JL, Pielak GJ (1995) Biochemistry 34:3140–3143
21. Santucci R, Bongiovanni C, Mei G, Ferri T, Polizio F, Desideri A (2000) Biochemistry 39:12632–12638
22. Wilgus H, Ranweiler JS, Wilson GS, Stellwagen E (1978) J Biol Chem 253:3265–3272
23. Wallace CJ (1987) J Biol Chem 262:16767–16770
24. Fisher A, Taniuchi H (1992) Arch Biochem Biophys 296:1–16
25. Kang X, Carey J (1999) J Mol Biol 285:463–468
26. Yokota A, Takenaka H, Oh T, Noda Y, Segawa S-I (1998) Protein Sci 7:1717–1727
27. Santucci R, Fiorucci L, Sinibaldi F, Polizio F, Desideri A, Ascoli F (2000) Arch Biochem Biophys 379:331–336
28. Santoni E, Scatragli S, Sinibaldi F, Fiorucci L, Santucci R, Smulevich G (2004) J Inorg Biochem 98:1067–1077
29. Sinibaldi F, Fiorucci L, Mei G, Ferri T, Desideri A, Ascoli F, Santucci R (2001) Eur J Biochem 268:4537–4543
30. Bushnell GW, Louie GV, Brayer GD (1990) J Mol Biol 214:585–595
31. Leszcynski JF, Rose GD (1986) Science 234:849–855
32. Pettigrew GW, Moore GR (1987) Cytochromes c. Biological aspects. Springer, Berlin Heidelberg New York
33. Jemmerson R, Liu J, Hausauer D, Lam K-P, Mondino A, Nelson RD (1999) Biochemistry 38:3599–3609
34. Sinibaldi F, Piro MC, Howes BD, Smulevich G, Ascoli F, Santucci R (2003) Biochemistry 42:7604–7610
35. Hoang L, Maity H, Krishna MMG, Lin Y, Englander SW (2003) J Mol Biol 331:37–43
36. Korszun ZN, Salemme FR (1977) Proc Natl Acad Sci USA 74:5244–5247
37. Eddowes MJ, Hill HAO (1979) J Am Chem Soc 101:4461–44641
38. Berghuis AM, Brayer GD (1992) J Mol Biol 223:959–976
39. Hoard JL (1973) Ann NY Acad Sci 206:18–31
40. Spaulding LD, Chang CC, Yu NT, Felton RH (1975) J Am Chem Soc 97:2517–2525
41. Choi S, Spiro TG, Langry KC, Smith KM, Budd DL, La Mar GN (1982) J Am Chem Soc 104:4345–4351
42. Sparks LD, Anderson KK, Medforth CJ, Smith K, Shelnutt JA (1994) Inorg Chem 33:2297–2302
43. Indiani C, De Sanctis G, Neri F, Santos H, Smulevich G, Coletta M (2000) Biochemistry 39: 8234–8242
44. Dopner S, Hildebrandt P, Rosell FI, Mauk AG (1998) J Am Chem Soc 120:11246–11255
45. Hu S, Morris IK, Singh JP, Smith KM, Spiro TG (1993) J Am Chem Soc 115:12446–12458
46. Smulevich G, Bjerrum MJ, Gray HB, Spiro TG (1994) Inorg Chem 33:4629–4634
47. Zheng J, Ye S, Lu T, Cotton TM, Chumanov G (2000) Biopolymers (Biospectroscopy) 57:77–84
48. Clark WM (1972) Oxidation-reduction potentials of organic systems. Krieger, Huntington, NY, USA
49. Santucci R, Reinhard H, Brunori M (1988) J Am Chem Soc 110:8536–8537
50. Raphael AL, Gray HB (1989) Proteins 6:338–340
51. Raphael AL, Gray HB (1991) J Am Chem Soc 113:1038–1040
52. Pielak GJ, Oikawa K, Mauk AG, Smith M, Kay CM (1986) J Am Chem Soc 108:2724–2727
53. Ascoli F, Santucci R (1996) J Inorg Biochem 68:211–214
54. Wilson MT, Greenwood C (1996) In: Scott RA, Mauk AG (eds), Cytochrome *c*. A multidisciplinary approach. University Science Books, Sausalito, Calif., USA, pp 611–634

55. Stellwagen E, Cass R (1974) Biochem Biophys Res Commun 60:371–375
56. Pace CN (1975) CRC Crit Rev Biochem: 1–43
57. Myers JK, Pace CN, Scholtz JM (1995) Protein Sci 4:2138–2148
58. Ferri T, Poscia A, Ascoli F, Santucci R (1996) Biochim Biophys Acta 1298:102–108
59. Nelson CJ, Bowler BE (2000) Biochemistry 39:13584–13594
60. Neri F, Indiani C, Welinder KG, Smulevich G (1998) Eur J Biochem 251:830–838
61. Wallace CJ, Proudfoot AE (1987) Biochem J 245:773–779
62. Guex N, Peitsch MC (1997) Electrophoresis 18:2714–2723